Overriding plate thickness as a controlling factor for trench retreat rates in narrow subduction zones

Pedro J. Gea[1], Flor de Lis Mancilla[1], Ana M Negredo[2], and Jeroen van Hunen[3]

[1]Universidad de Granada
[2]Universidad Complutense de Madrid
[3]Durham University

March 26, 2023

Abstract

Slab width plays a major role in controlling subduction dynamics and trench motion. However, observations on natural narrow subduction zones do not show any correlation between slab width and trench velocities, indicating that other factors may have a greater impact. Here, we use 3D numerical subduction models to evaluate the effect of slab width, strength of slab coupling to the lateral plate and overriding plate thickness on trench kinematics. Model results show that slab width has little influence on trench migration rates for narrow subduction zones, but that the thickness of the overriding plate plays a major role, with trench velocities decreasing as the thickness increases. These results explain trench velocities observed in natural narrow subduction zones showing no relation with slab width but an inverse dependence on overriding plate thickness. Finally, we find that the overriding plate thickness also significantly affects the trench shape.

Overriding plate thickness as a controlling factor for trench retreat rates in narrow subduction zones

Pedro J. Gea[1,2], Flor de Lis Mancilla[1,2], Ana M. Negredo[3,4], and Jeroen van Hunen[5]

[1]Department of Theoretical Physics and Cosmology, University of Granada, Granada, Spain
[2]Andalusian Institute of Geophysics, University of Granada, Granada, Spain
[3]Department of Earth Physics and Astrophysics, Complutense University of Madrid, Madrid, Spain
[4]Institute of Geosciences IGEO (CSIC, UCM), Madrid, Spain
[5]Department of Earth Sciences, Durham University, DH1 3LE Durham, UK

Key Points:

- Three-dimensional numerical models of narrow subduction zones including all plates are performed to study trench kinematics
- Overriding plate thickness is the main factor affecting trench retreat velocities in narrow subduction zones
- The overriding plate has an important role in modulating trench geometries

Corresponding author: Pedro J. Gea, `pedrog@ugr.es`

Abstract

Slab width plays a major role in controlling subduction dynamics and trench motion. However, observations on natural narrow subduction zones do not show any correlation between slab width and trench velocities, indicating that other factors may have a greater impact. Here, we use 3D numerical subduction models to evaluate the effect of slab width, strength of slab coupling to the lateral plate and overriding plate thickness on trench kinematics. Model results show that slab width has little influence on trench migration rates for narrow subduction zones, but that the thickness of the overriding plate plays a major role, with trench velocities decreasing as the thickness increases. These results explain trench velocities observed in natural narrow subduction zones showing no relation with slab width but an inverse dependence on overriding plate thickness. Finally, we find that the overriding plate thickness also significantly affects the trench shape.

Plain Language Summary

Subduction zones are the main drivers of plate tectonics and control much of the seismic and volcanic activity on Earth. For that reason, subduction processes have been widely studied in the last few decades. Because of the limited amount of available data, one of the key techniques has been numerical modelling. Some earlier models have shown that the velocity of the trench (long region marking where subduction starts) is affected by the width of the subduction zone, but this is not observed for narrow subduction zones in nature. In this work, we model 3D narrow subduction systems and find that the thickness of the unsubducted overriding plate affects trench velocities much more than the width of the subduction zone: the thicker the plate, the slower the trench motion. Moreover, the thickness of the overriding plate affects the shape that the trench develops. Our models explain some key observations in Earth's narrow subduction zones and help to better understand these processes.

1 Introduction

Subducting slabs are the main drivers of plate motion and flow in Earth's mantle. Thus, much effort has been put in the last few decades into understanding the main factors controlling slab dynamics and subduction-induced mantle flow (e.g., Billen, 2008; Funiciello et al., 2003; Gerya, 2022; Schellart, 2004; Stegman et al., 2010; van Hunen & Allen, 2011). Previous geodynamic modelling studies have shown the wide variety of physical parameters that influence subduction processes, such as the slab thickness (Bellahsen et al., 2005; Capitanio & Morra, 2012; F. Chen et al., 2022; Funiciello et al., 2008; Stegman et al., 2010) and length (A. F. Holt & Becker, 2016; Xue et al., 2020), the mantle rheology (A. F. Holt & Becker, 2016; Pusok et al., 2018), the strength and thickness of the overriding plate (OP) (Butterworth et al., 2012; Hertgen et al., 2020; A. Holt et al., 2015; Meyer & Schellart, 2013; Rodríguez-González et al., 2014; Sharples et al., 2014), the slab-mantle viscosity contrast (Funiciello et al., 2008; Schellart, 2008; Stegman et al., 2010), the coupling at the subduction-interface (Čížková & Bina, 2013, 2019; Behr et al., 2022) or the mechanical boundary conditions (Z. Chen et al., 2015; Funiciello et al., 2004). All these studies highlight the complexity of subduction, which makes these processes still incompletely understood in their key aspects (Gerya, 2022).

Among the factors controlling subduction dynamics, the slab width (W) has been shown to be of major importance (Bellahsen et al., 2005; F. Chen et al., 2022; Di Giuseppe et al., 2008; Guillaume et al., 2010, 2021; Royden & Husson, 2006; Schellart et al., 2007; Stegman et al., 2006, 2010; Strak & Schellart, 2016). Earlier geodynamic studies have distinguished three types of trench curvature depending on slab width: concave for narrow slabs (W $\leq$ 1500 km), "w"-shaped (also referred to as sublinear) for intermediate width slabs (W $\sim$ 2000-3000 km) and convex for wide slabs (W $\geq$ 4000 km) (Schellart et al., 2007; Stegman et al., 2010; Strak & Schellart, 2016), although the exact values differentiating these regimes depend somewhat on the specific conditions. In addition, the slab dip seems to be controlled by W, increasing (producing steeper slabs) with wider subducting plates (Schellart, 2004; Strak & Schellart, 2016). W also controls the subduction-induced mantle flow (Piromallo et al., 2006; Stegman et al., 2006), causing faster and more localized mantle upwellings near the lateral slab edges for wider slabs (Strak & Schellart, 2016). Regarding the slab kinematics, previous studies have shown that the trench retreat velocity (V_T) decreases as the slab becomes wider (F. Chen et al., 2022; Schellart, 2004; Schellart et al., 2007; Stegman et al., 2006). All these studies provide useful insights that help to understand the effect of W on subduction processes. However, most of these model setups that specifically focused on slab width had no OP, which is known to affect subduction dynamics significantly (e.g., Hertgen et al., 2020; Magni et al., 2014; Yamato et al., 2009). Additionally, the inverse depencence of V_T on W predicted by some models is not observed in natural narrow subduction zones (e.g., Calabria, Gibraltar, Scotia), which do not show any correlation between W and V_T, suggesting that other factors may play a more relevant role on trench retreat velocities. Incorporating an OP can help to better understand the effect of W on V_T and the dominant factors controlling trench retreat rates in narrow subduction zones.

In this study, we have conducted self-consistent 3D numerical subduction models to systematically evaluate in narrow subduction zones the effect of slab width, overriding plate thickness and coupling of the slab with the lateral plate on trench motion. In order to model realistic subduction processes, we have included the subducting and surrounding plates (lateral and overriding). Based on our geodynamic models and a comparison with observations in nature, this work explores the factors dominating trench retreat velocities in narrow subduction zones and provides new insights on the role of the OP in trench motion.

2 Methods

The simulations have been performed with version 2.4.0 of the finite-element code ASPECT (Advanced Solver for Problems in Earth's ConvecTion) (Kronbichler et al., 2012; Heister et al., 2017; Gassmöller et al., 2018; Bangerth et al., 2021a, 2021b). We have used the Boussinesq approximation to solve the coupled conservation equations for mass, momentum and energy, which assumes that the density is constant in all equations except in the buoyancy term of the momentum equation (Text S1 in the supporting information).

The initial 3-D model setup is shown in Figure 1. The initial geometry has been built using the Geodynamic World Builder (GWB) version 0.4.0 (Fraters et al., 2019, 2021) and it measures 2000x800x660 km in the x, y and z directions. Because the XZ plane at y = 0 is a plane of symmetry (Figure 1), we only model one half of the subduction zone. The initial geometry consists of an ongoing subduction system with a 220 km-long slab and a dip angle of 40°. In this way, the model is self-driven by buoyancy and the rest of internal forces. The subducting plate (SP) is comprised of weak crust 10 km thick and lithospheric mantle 85 km thick. The weak crust allows for the decoupling of the slab from the top surface and from the OP to facilitate subduction. The SP width is varied between models in the range of 400-1200 km. The OP has an initial thickness of 70 km, consisting of a 30 km crust and a 40 km lithospheric mantle, although its thickness also varies between models. The lateral plate (LP) is completely made of lithosphere 95 km thick, without any compositional stratification. We use a zone 20 km wide (transform fault) as a mechanical coupling of the lateral plate with the other plates. The trench is initially located at x = 1000 km, and we use particles placed along its length to track its movement over the time. The inclusion of the OP and LP provides a reasonable model setup and avoids unrealistic behaviour since the presence of these plates strongly affects the subduction dynamics (e.g., Yamato et al., 2009). For example, previous studies have shown that the presence of an OP results in a slowdown of the trench retreat velocities, highlighting that the poloidal flow is affected by the coupling of the subducting and overriding plate (e.g., Capitanio et al., 2010; Yamato et al., 2009). Regarding the role of the LP, its inclusion in subduction models prevents lateral shortening (Yamato et al., 2009).

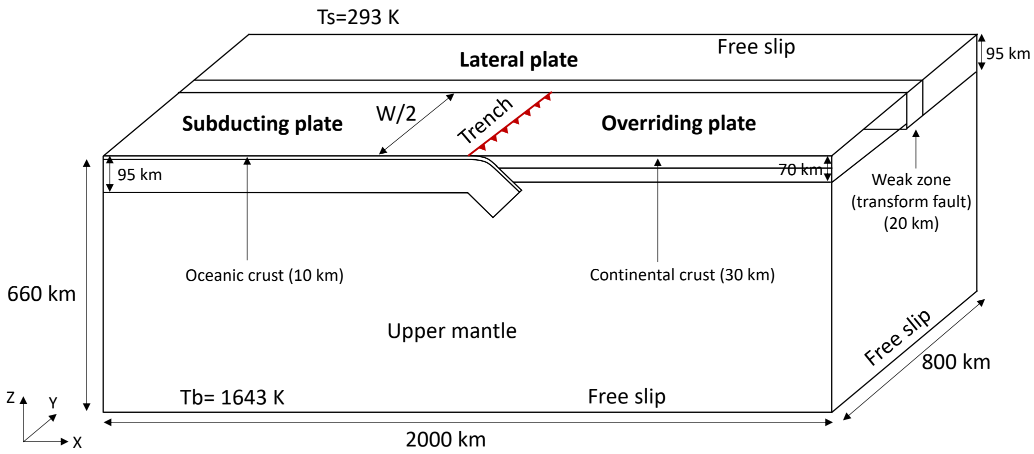

Figure 1. Three-dimensional model setup and boundary conditions. The setup includes a subducting plate (SP), an overriding plate (OP) and a lateral plate (LP). W indicates slab width and the red line with triangles marks the initial trench position at x = 1000 km. The trench is plotted for the whole subduction zone in Figures 2 and 3. The temperature is fixed to 293 K at the top boundary and 1643 K at the bottom boundary. All boundaries are free slip. Note that only half of the subduction zone is modelled due to the symmetry of the problem.

The initial temperature profile increases linearly from 293 K at the surface to 1643 K at the lithosphere-asthenosphere boundary (LAB). For the top and bottom boundaries we use Dirichlet temperature conditions. All boundaries are free slip, which means that the velocity perpendicular to the boundaries is prescribed to 0 (Dirichlet boundary condition) and that there are no stresses parallel to the boundary (Neumann boundary condition). In terms of rheology, we use a temperature-dependent viscosity (Text S2 and Table S1 in the supporting information) except for the subducting plate crust and weak zone where we impose constant viscosities of 10^{20} Pa s. With this rheology, we obtain a viscosity of $1.57 \cdot 10^{20}$ Pa s at a depth of 150 km. Finally, we impose cutoffs of $1 \cdot 10^{19}$ and $1.57 \cdot 10^{23}$ Pa s (1000 times the upper mantle viscosity at a depth of 150 km) to avoid large viscosity jumps. All model parameters are listed in Table S1 in the supporting information.

3 Results

3.1 Effect of slab width and coupling at the lateral slab edge

In order to study narrow subduction zones, we performed experiments varying W in the range of 400 to 1200 km. For each experiment, we have tested different amounts of mechanical coupling of the slab with the lateral plate by changing the viscosity of the transform fault (μ_{TF}) (experiments 1-15, Table S2 in the supporting information).

The subduction dynamics is similar in all the experiments. Initially, the slab freely sinks into the upper mantle due to the density contrast and the trench retreat velocities quickly increase (Figure 2d), accompanied by slab rollback and inducing toroidal flow around the slab edges (Figure S1 in the supporting information). All models show the maximum V_T when the slab tip reaches ∼400 km depth. Thereafter, trench velocities slightly decrease due to the interaction of the slab tip with the deep viscous upper mantle, and approach a roughly constant value (Figure 2d).

Figures 2a-2d show the trench kinematics for a weak slab coupling to the lateral plate (μ_{TF} = 10^{20} Pa s). Models develop two types of trench geometries in the center of the subduction zone depending on W. The trench in models with W $\leq$ 1000 km shows a concave geometry toward the overriding plate, with the trench in the center of the subduction zone retreating faster than its edges (Figures 2a and 2b). This characteristic geometry is attained earlier in models with smaller W. For example, the concave geometry for W = 400 km is almost achieved in 2 Myr, while for W = 600 km it is not attained until 10 Myr. For the model with W = 1200 km, the trench geometry is rectilinear in its center up to 10 Myr, and thereafter adopts a "w"-shape, with retreat velocities being higher in between the lateral slab edge and the center of the subduction zone (Figure 2c). The highest V_T is found for W = 600 km and decreases for wider slabs (Figure 2d and blue line in Figure 2e).

Concerning the mechanical coupling of the slab with the lateral plate, we find that the maximum V_T correlates positively with W for W $\leq$ 600 km when the viscosity of the transform fault is $\mu_{TF} = 10^{20}$ Pa s, but for W $\leq$ 800 km when $\mu_{TF} = 10^{21}$ or $\mu_{TF} = 10^{22}$ Pa s (Figure 2e). The maximum V_T decreases as the viscous coupling increases for W $\leq$ 800 km, but does not change significantly for W $>$ 800 km. The fact that the three curves in Figure 2e tend to converge with W approaching 1200 km indicates that effect of the strength of lateral coupling on V_T is only significant for very narrow subduction zones, and give maximum V_T differences about 1.8 cm/yr for W = 400 km. Finally, increasing the viscous coupling to the lateral plate also results in more concave trench geometries. For a W of 1200 km, we obtain "w"-shapes for $\mu_{TF} = 10^{20}$ and $\mu_{TF} = 10^{21}$ Pa s and concave geometries for $\mu_{TF} = 10^{22}$ Pa s (Figure S2 in the supporting information).

3.2 Effect of overriding plate thickness

We have varied the overriding plate thickness in the range of 40 to 100 km to study its effect on trench motion (experiments 2 and 16-21, Table S2 in the supporting information). In our models, the trench develops a concave geometry in all cases (Figures 3a, 3c and 3d) except for an OP thickness of 100 km, where a "w"-shape develops after about 10 Myr of evolution (Figure 3b), showing that thick overriding plates facilitates the formation of such geometries. Significant trench lateral shortening is also observed as the OP thickness increases (Figures 3b and 3d). Regarding the kinematics, V_T significantly decreases with thicker overriding plates (Figure 3e). For example, the maximum V_T is $\sim$ 6.8 cm/yr with an OP 40 km thick and decreases to $\sim$ 5.4 cm/yr with an OP 60 km thick. Short periods of small trench advance at the beginning of the simulation occur for OP thicknesses greater than 70 km (Figure 3e).

4 Discussion

4.1 Comparison with previous studies

Our geodynamic models provide new insights into the effect of W, OP thickness and strength of slab coupling to the lateral plate on trench kinematics. We find two out of the three types of trench geometries identified by Schellart et al. (2007), Stegman et al. (2010) and Strak and Schellart (2016) but for a different range of W values. The numerical models of Schellart et al. (2007) and Stegman et al. (2010) suggest values of W $\leq$ 1500 km, W $\sim$ 2000-3000 km and W $\geq$ 4000 km leading to concave, "w"-shaped and convex trenches, while the analog models of Strak and Schellart (2016) indicate values of W = 2000-2500 km and W $\geq$ 3000 km for "w"-shaped and convex geometries respectively. The analog modelling of Guillaume et al. (2021) predicts concave and "w"-shaped geometries even for wider slabs (W = 2000 and W = 4000 km respectively). Similarly, the recent 3-D spherical shell numerical models of F. Chen et al. (2022) place the transition from concave trenches to "w"-shaped geometries at a W of 2400 km for their reference case. Our results do not show convex geometries, which is expected as we focus only on narrow subduction zones and these geometries are found for very wide slabs (Schellart et al., 2007; Strak & Schellart, 2016). However, our models show a "w"-shaped geometry for a much narrower slab (W = 1200 km, Figure 2c) than in previous studies (W $\geq$ 2000). Following our results, a likely factor

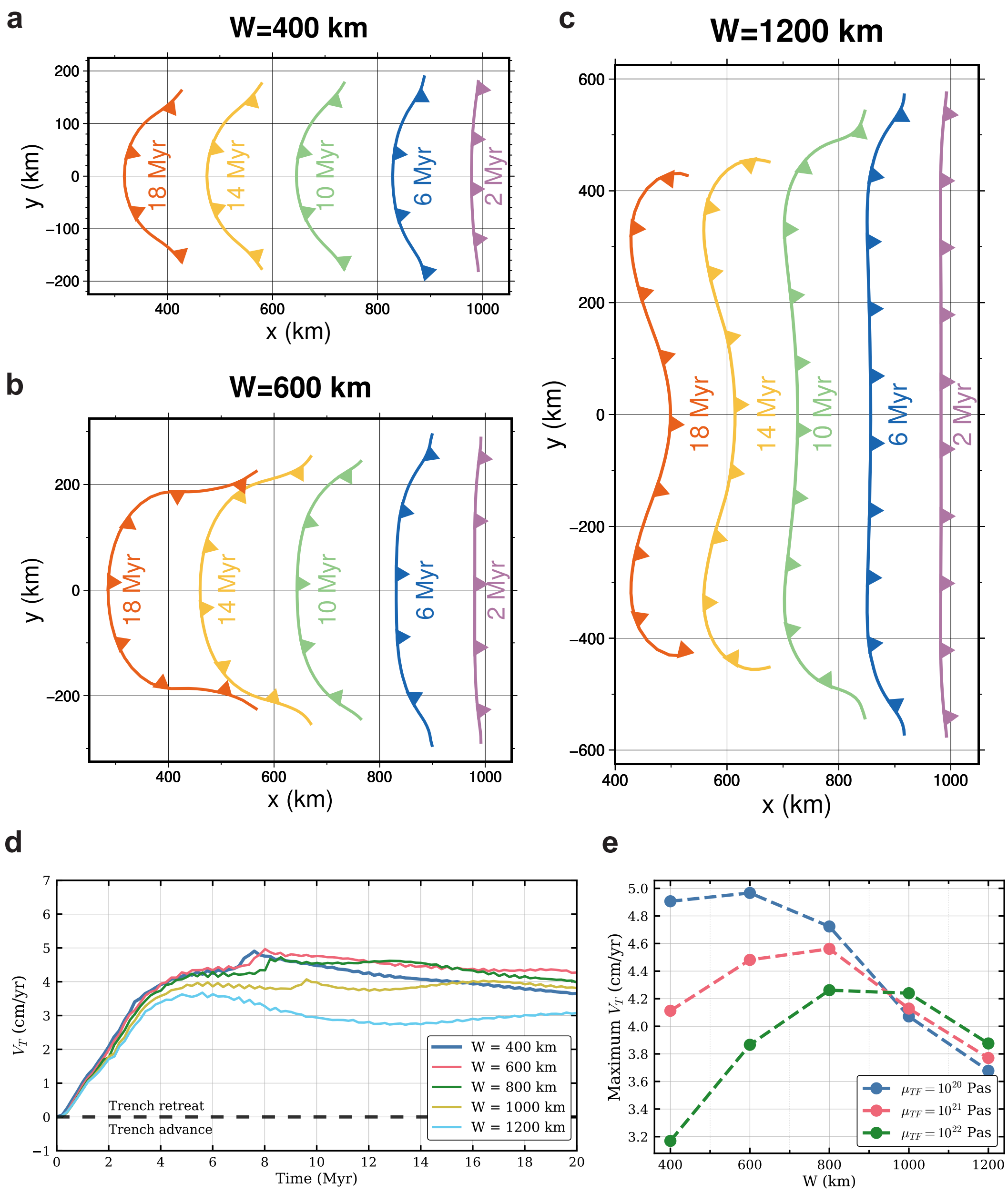

Figure 2. (a-c) Evolution of the subduction trench for three simulations with (a) W = 400 km, (b) W = 600 km and (c) W = 1200 km. Note that the entire trench is plotted but we only model half of the subduction zone. (d) V_T over time (measured in the center of the subduction zone) for simulations with different W. Panels (a-d) show the results for a $\mu_{TF} = 10^{20}$ Pa s. (e) Maximum V_T at the center of the subduction zone for diferrent W and different viscous coupling at the lateral slab edge.

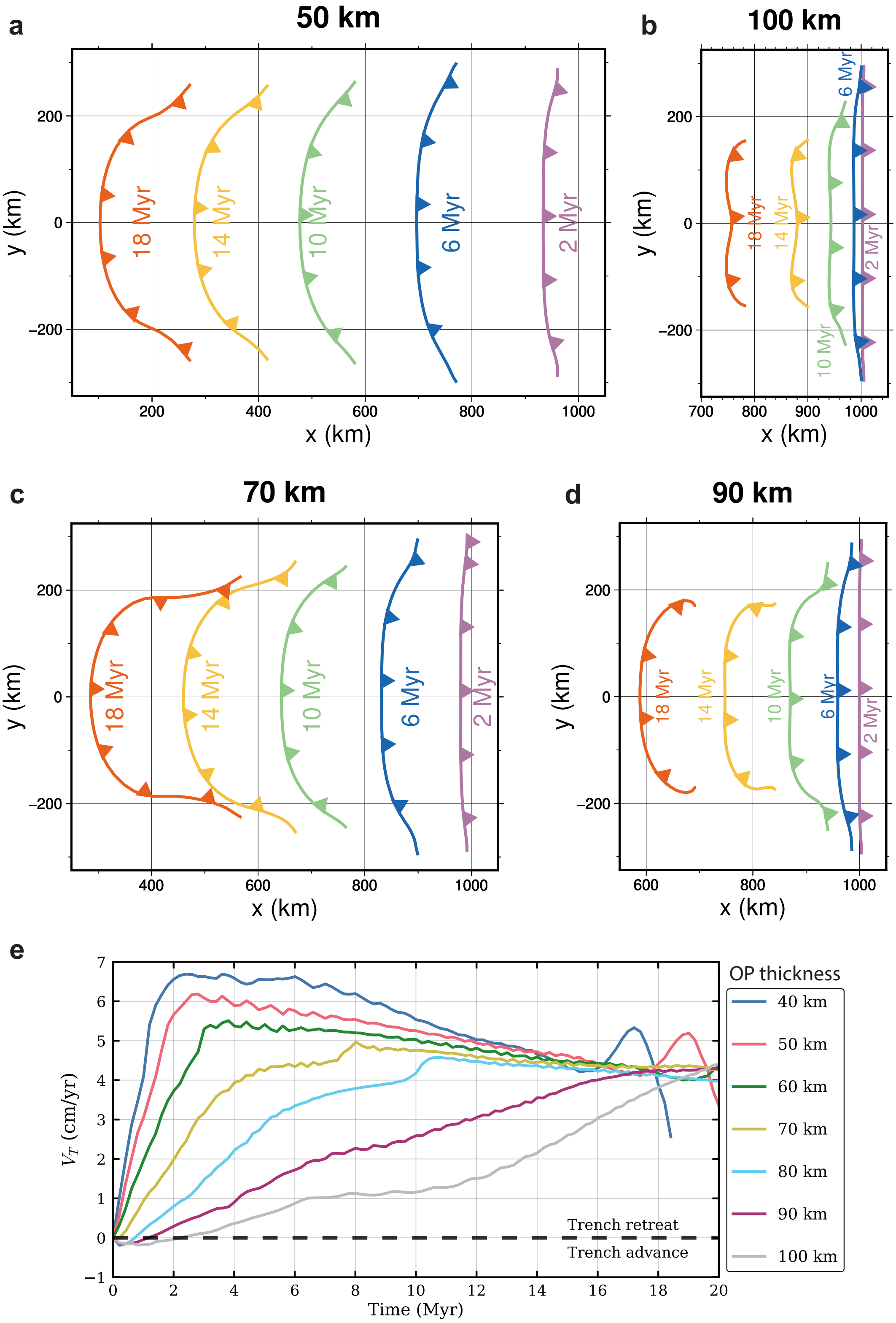

Figure 3. (a-d) Evolution of the subduction trench for four simulations with OP thicknesses of (a) 50 km, (b) 100 km, (c) 70 km and (d) 90 km. Note that the entire trench is plotted but we only model half of the subduction zone. (e) V_T over time (measured in the center of the subduction zone) for simulations with different OP thicknesses.

that could explain these discrepancies is the influence of the OP, which was not included in such previous studies. In fact, our results show that increasing the OP thickness in models with the same W leads to "w"-shaped trenches (Figure 3b).

Regarding trench migration velocities, previous modelling studies have found that V_T decreases with increasing W (e.g., F. Chen et al., 2022; Schellart et al., 2007; Stegman et al., 2006). However, this behaviour is not always maintained for narrow subduction zones. Our results show a direct dependence of V_T on W for W $\leq$ 600 km when the mechanical coupling of the slab with the lateral plate is weak ($\mu_{TF} = 10^{20}$ Pa s) and for W $\leq$ 800 km when the coupling is stronger ($\mu_{TF} = 10^{21}$ and $\mu_{TF} = 10^{22}$ Pa s) (Figure 2e). This positive correlation between V_T and W has also been suggested in previous works for W $\leq$ 500-600 km (Schellart, 2004; Stegman et al., 2006) and for W $\leq\sim$ 1000 km (Strak & Schellart, 2016). Our models using a weak coupling are in agreement with the results of Stegman et al. (2006) finding a maximum retreat velocity for W = 600 km. The difference between the present work and previous studies on which slab width exhibits the highest V_T suggests a dependence on different model parameters and setup. For example, our models show that the W for which V_T peaks increases as the viscous coupling at the transform fault becomes stronger (Figure 2e). More research is needed to clarify the dynamics and factors affecting this phenomenon. Here we propose that a peak V_T is observed in Figure 2e due to an energy balance (Magni et al., 2014) between the available gravitational potential energy of the slab E_{pot} and the energy required for frictional dissipation in the mantle $E_{diss,m}$ and at the transform fault $E_{diss,TF}$. For relatively wide slabs, $E_{diss,TF}$ is relatively unimportant, E_{pot} linearly increases with slab width, while $E_{diss,m}$ increases faster than that. So trench retreat is slower for wider slabs. For narrow slabs, E_{pot} and $E_{diss,m}$ are both small, and $E_{diss,TF}$ becomes more important. Since E_{pot} decreases for narrowing slabs, while $E_{diss,TF}$ is independent of slab width, narrow slabs retreat slower than wider slabs. Finally, our models demonstrate the strong impact of the OP thickness on trench retreat velocities, with V_T decreasing significantly with increasing OP thickness (Figure 3e). This result is in agreement with the recent 3D numerical modelling including a SP and OP by Hertgen et al. (2020), who found that thin/weak OP favours faster trench velocities and rollback compared to a thick/strong OP. The 2D self-consistent subduction models of Gea et al. (2023) and A. Holt et al. (2015) also show that a thicker OP leads to a reduction in V_T. Increasing the thickness of the OP limits the space for the induced mantle to flow beneath it, thus reducing the interaction between the slab and the poloidal flow and resulting in lower trench retreat.

4.2 Comparison with nature

Natural subduction zones on Earth are influenced by a large number of factors that are not included in our models, such as slabs of non-uniform age, complex slab morphologies or plate velocities. Thus, comparing our results with observations on Earth should be approached with caution, being aware of the inherent limitations. Nevertheless, our geodynamic model predictions are useful to explain some observations on natural narrow subduction zones.

The concave trench geometries predicted by our geodynamic models are widely observed on Earth for narrow subduction zones. The Gibraltar slab is the clear example of this geometry (Figure 4a). Our results have demonstrated that including an OP facilitates the formation of "w"-shaped geometries. For example, our model with W = 1200 km and $\mu_{TF} = 10^{20}$ Pa s develops a "w"-shape (Figure 2c) for much smaller W than any of the previous studies not using an OP (e.g., F. Chen et al., 2022; Schellart et al., 2007; Stegman et al., 2010; Strak & Schellart, 2016). Increasing the thickness of the OP has also been shown to affect the geometry of the trench, with a OP 100 km thick leading to a "w"-shaped geometry (Figure 3b). This effect of the OP could explain why some natural subduction zones of narrow to intermediate widths develop "w"-shapes. For example, the Manila trench (W = 1000 km) has a geometry between concave and "w"-shaped (Figure

4c) and the Hellenic Arc (W = 1700 km) shows a clear "w"-shape (Figure 4b), with a much narrower W than those predicted by previous studies not including an OP.

The decrease in V_T with increasing W observed in the present work for W $\geq$ 800 km (Figures 2d and 2e) and in previous works (e.g., F. Chen et al., 2022; Royden & Husson, 2006; Schellart et al., 2007; Stegman et al., 2006) is in general agreement with observations in narrow and wide subduction zones. This result explains why narrow subduction zones (e.g. Calabria, South Shetland, Halmahera) exhibit relatively high V_T, while wide subduction zones (e.g. Melanesia, South America) are essentially stationary (Schellart et al., 2007). However, when this comparison is restricted to narrow subduction zones, no such correlation is observed (Figure 4d). For the same slab width ($\sim$ 900 km), the Makran subduction zone has a V_T of 0.2 cm/yr while the Trobriand system has a V_T of 7.6 cm/yr. Our results showing that W has little effect on V_T for narrow subduction zones, with variations in $V_T \leq 1$ cm/yr (Figure 2e), are in agreement with the lack of correlation between W and V_T observed in nature and provide an explanation for these observations. In contrast, our models reveal that the effect of OP thickness is much stronger, showing an inverse dependence of V_T on OP thickness (Figure 3e). This tendency is also observed in nature for narrow subduction zones (Figure 4e) and brings an explanation of why two subduction zones with the same W (such as Makran and Trobriand) show such different V_T.

5 Conclusions

The 3-D numerical subduction models presented in this work shed light on some factors (slab width, overriding plate thickness and coupling of the slab with the lateral plate) controlling trench kinematics in narrow subduction zones, and help to explain some observations of natural subduction processes. As opposed to what happens in wide subduction zones, our models show that the slab width has little effect on trench retreat velocities for narrow subduction zones, which is consistent with the lack of correlation between these parameters observed in nature. In contrast, from our models and observations in nature we conclude that the thickness of the overriding plate is the main controlling factor on trench retreat velocities for narrow subduction zones, with velocities decreasing as the thickness increases. The strength of slab coupling to the lateral plate is only significant for very narrow subduction zones. Finally, the inclusion of an overriding plate plays an important role in modulating trench geometries, facilitating the formation of "w"-shaped geometries, which are predicted for smaller slab widths than in previous studies.

6 Open Research

The version 2.4.0 of ASPECT used in this study is available at `https://zenodo.org/record/6903424`. All the information and parameters of the models of this work can be found in the Methods section, in Text S1 and S2 in the supporting information and in Table S1 in the supporting information. The files required to reproduce our simulations are available on `https://github.com/Pedrogea08/Gea_et_al_2023GRL`.

Acknowledgments

This work has been funded by Spanish Ministry of Science and Innovation projects PID 2019-109608GB-I00, PGC 2018-095154-B-I00 and PID 2020-114854GB-C22 and FEDER-Junta de Andalucia-Conserjeria de Economia y Conocimiento/B-RNM-528-UGR20. The computing time was provided by the the Centro de Servicios de Informática y Redes de Comunicación (CSIRC), Universidad de Granada and by the Hamilton HPC cluster, University of Durham. We also thank the Computational Infrastructure for Geodynamics (geodynamics.org) which is funded by the National Science Foundation under award EAR-0949446 and EAR-1550901 for supporting the development of ASPECT.

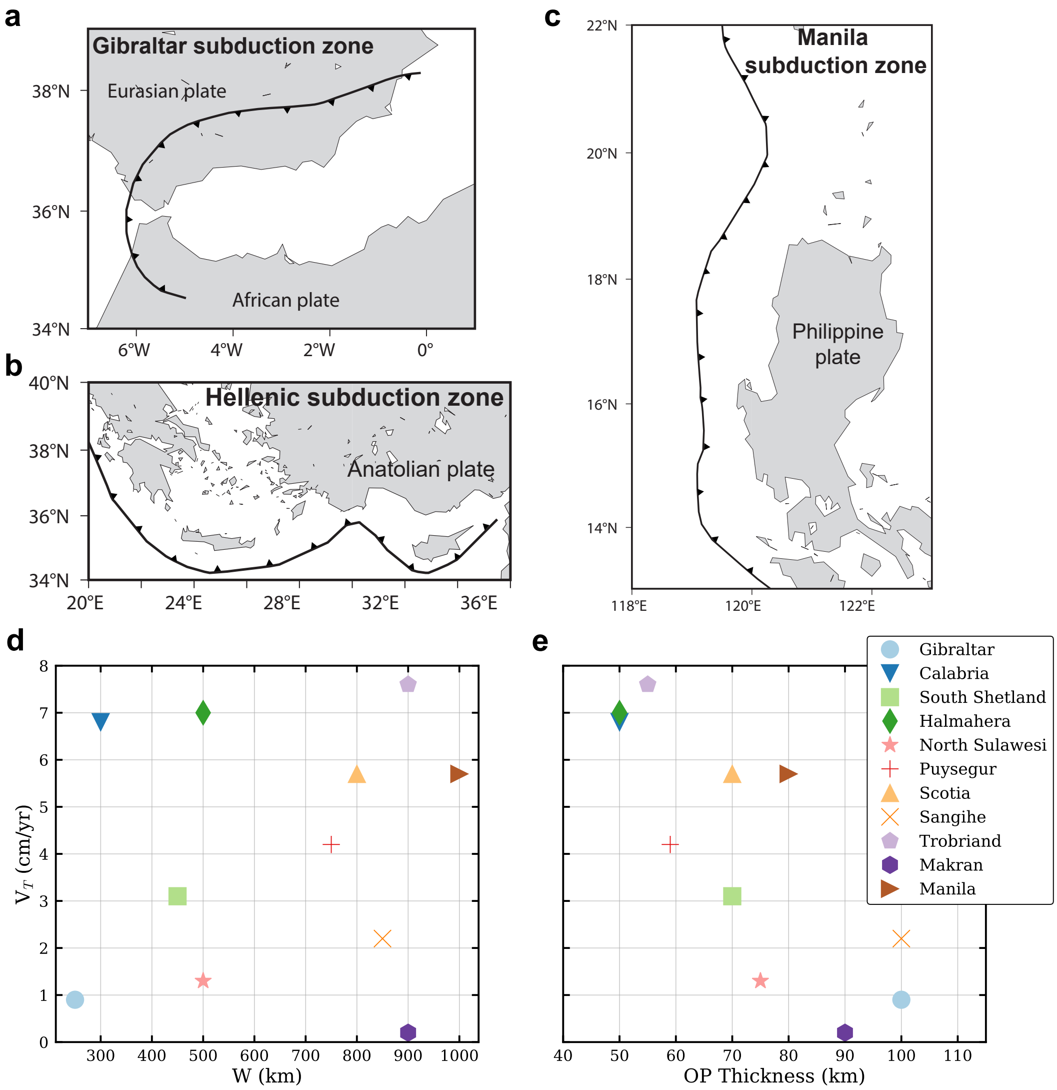

Figure 4. (a-c) Subduction fronts at present-day for the (a) Gibraltar subduction system (from Gutscher et al. (2012), (b) Hellenic subduction zone (from Lemenkova (2021)) and (c) Manila subduction zone (from Qiu et al. (2019)). (c) V_T against W for all subduction zones in Earth with W $\leq$ 1000 km (data from Schellart et al. (2007)). (e) V_T against OP thickness for all subduction zones in Earth with W $\leq$ 1000 km (data can be found in table S3 in the supporting information).

References

Bangerth, W., Dannberg, J., Fraters, M., Gassmoeller, R., Glerum, A., Heister, T., & Naliboff, J. (2021a, July). ASPECT*: Advanced Solver for Problems in Earth's ConvecTion, User Manual.* doi: 10.6084/m9.figshare.4865333

Bangerth, W., Dannberg, J., Fraters, M., Gassmoeller, R., Glerum, A., Heister, T., & Naliboff, J. (2021b, July). *Aspect v2.4.0-pre.* Zenodo. doi: 10.5281/zenodo.5131909

Behr, W. M., Holt, A. F., Becker, T. W., & Faccenna, C. (2022, 02). The effects of plate interface rheology on subduction kinematics and dynamics. *Geophysical Journal International*, *230*(2), 796-812. doi: 10.1093/gji/ggac075

Bellahsen, N., Faccenna, C., & Funiciello, F. (2005). Dynamics of subduction and plate motion in laboratory experiments: Insights into the "plate tectonics" behavior of the earth. *Journal of Geophysical Research: Solid Earth*, *110*(B1). doi: 10.1029/2004JB002999

Billen, M. I. (2008). Modeling the dynamics of subducting slabs. *Annual Review of Earth and Planetary Sciences*, *36*(1), 325-356. doi: 10.1146/annurev.earth.36.031207.124129

Butterworth, N., Quevedo, L., Morra, G., & Müller, D. (2012, 06). Influence of overriding plate geometry and rheology on subduction. *Geochemistry, Geophysics, Geosystems*, *13*, Q06W15. doi: 10.1029/2011GC003968

Capitanio, F., & Morra, G. (2012). The bending mechanics in a dynamic subduction system: Constraints from numerical modelling and global compilation analysis. *Tectonophysics*, *522-523*, 224-234. doi: 10.1016/j.tecto.2011.12.003

Capitanio, F., Stegman, D., Moresi, L., & Sharples, W. (2010, 03). Upper plate controls on deep subduction, trench migrations and deformations at convergent margins. *Tectonophysics*, *483*, 80-92. doi: 10.1016/j.tecto.2009.08.020

Chen, F., Davies, D. R., Goes, S., Suchoy, L., & Kramer, S. C. (2022). How slab age and width combine to dictate the dynamics and evolution of subduction systems: A 3-d spherical study. *Geochemistry, Geophysics, Geosystems*, *23*(11), e2022GC010597. doi: 10.1029/2022GC010597

Chen, Z., Schellart, W., & Duarte, J. (2015, 10). Overriding plate deformation and variability of fore-arc deformation during subduction: Insight from geodynamic models and application to the calabria subduction zone. *Geochemistry Geophysics Geosystems*. doi: 10.1002/2015GC005958

Di Giuseppe, E., van Hunen, J., Funiciello, F., Faccenna, C., & Giardini, D. (2008). Slab stiffness control of trench motion: Insights from numerical models. *Geochemistry, Geophysics, Geosystems*, *9*(2). doi: 10.1029/2007GC001776

Fraters, M., et al. (2021, July). *The Geodynamic World Builder v0.4.0.* Zenodo. (Zenodo. doi:10.5281/zenodo.5014808) doi: 10.5281/zenodo.5014808

Fraters, M., Thieulot, C., van den Berg, A., & Spakman, W. (2019). The Geodynamic World Builder: a solution for complex initial conditions in numerical modeling. *Solid Earth*, *10*(5), 1785–1807. doi: 10.5194/se-10-1785-2019

Funiciello, F., Faccenna, C., & Giardini, D. (2004, 06). Role of lateral mantle flow in the evolution of subduction systems: insights from laboratory experiments. *Geophysical Journal International*, *157*(3), 1393-1406. doi: 10.1111/j.1365-246X.2004.02313.x

Funiciello, F., Faccenna, C., Giardini, D., & Regenauer-Lieb, K. (2003). Dynamics of retreating slabs: 2. insights from three-dimensional laboratory experiments. *Journal of Geophysical Research: Solid Earth*, *108*(B4). doi: 10.1029/2001JB000896

Funiciello, F., Faccenna, C., Heuret, A., Lallemand, S., Di Giuseppe, E., & Becker, T. (2008). Trench migration, net rotation and slab–mantle coupling. *Earth and Planetary Science Letters*, *271*(1), 233-240. doi: 10.1016/j.epsl.2008.04.006

Gassmöller, R., Lokavarapu, H., Heien, E., Puckett, E. G., & Bangerth, W. (2018). Flexible and scalable particle-in-cell methods with adaptive mesh refinement for geodynamic computations. *Geochemistry, Geophysics, Geosystems*, *19*(9), 3596–3604. doi: 10.1029/2018GC007508

Gea, P. J., Negredo, A. M., & Mancilla, F. d. L. (2023). The gibraltar slab dynamics and its influence on past and present-day alboran domain deformation: Insights from thermo-mechanical numerical modelling. *Frontiers in Earth Science*, *11*. doi: 10.3389/feart.2023.995041

Gerya, T. (2022, 02). Numerical modeling of subduction: State of the art and future directions. *Geosphere*, *18*(2), 503-561. doi: 10.1130/GES02416.1

Guillaume, B., Funiciello, F., & Faccenna, C. (2021). Interplays between mantle flow and slab pull at subduction zones in 3d. *Journal of Geophysical Research: Solid Earth*, *126*(5), e2020JB021574. doi: 10.1029/2020JB021574

Guillaume, B., Funiciello, F., Faccenna, C., Martinod, J., & Olivetti, V. (2010, 09). Spreading pulses of the Tyrrhenian Sea during the narrowing of the Calabrian slab. *Geology*, *38*(9), 819-822. doi: 10.1130/G31038.1

Gutscher, M.-A., Dominguez, S., Westbrook, G., Le Roy, P., Rosas, F., Duarte, J., ... Bartolome, R. (2012). The gibraltar subduction: A decade of new geophysical data. *Tectonophysics*, *574-575*, 72-91. doi: 10.1016/j.tecto.2012.08.038

Heister, T., Dannberg, J., Gassmöller, R., & Bangerth, W. (2017). High accuracy mantle convection simulation through modern numerical methods. II: Realistic models and problems. *Geophysical Journal International*, *210*(2), 833-851. doi: 10.1093/gji/ggx195

Hertgen, S., Yamato, P., Guillaume, B., Magni, V., Schliffke, N., & van Hunen, J. (2020, 01). Influence of the thickness of the overriding plate on convergence zone dynamics. *Geochemistry, Geophysics, Geosystems*, *21*, e2019GC008678. doi: 10.1029/2019GC008678

Holt, A., Becker, T., & Buffett, B. (2015, 02). Trench migration and overriding plate stress in dynamic subduction models. *Geophysical Journal International*, *201*, 172-192. doi: 10.1093/gji/ggv011

Holt, A. F., & Becker, T. W. (2016, 10). The effect of a power-law mantle viscosity on trench retreat rate. *Geophysical Journal International*, *208*(1), 491-507. doi: 10.1093/gji/ggw392

Kronbichler, M., Heister, T., & Bangerth, W. (2012). High accuracy mantle convection simulation through modern numerical methods. *Geophysical Journal International*, *191*, 12-29. doi: 10.1111/j.1365-246X.2012.05609.x

Lemenkova, P. (2021, 09). Submarine tectonic geomorphology of the pliny and hellenic trenches reflecting the geological evolution of southern greece. *Rudarsko Geolosko Naftni Zbornik*, *36*, 33-48. doi: 10.17794/rgn.2021.4.4

Magni, V., Faccenna, C., van Hunen, J., & Funiciello, F. (2014, 06). How collision triggers backarc extension: Insight into Mediterranean style of extension from 3-D numerical models. *Geology*, *42*(6), 511-514. doi: 10.1130/G35446.1

Meyer, C., & Schellart, W. P. (2013). Three-dimensional dynamic models of subducting plate-overriding plate-upper mantle interaction. *Journal of Geophysical Research: Solid Earth*, *118*(2), 775-790. doi: 10.1002/jgrb.50078

Piromallo, C., Becker, T. W., Funiciello, F., & Faccenna, C. (2006). Three-dimensional instantaneous mantle flow induced by subduction. *Geophysical Research Letters*, *33*(8). doi: 10.1029/2005GL025390

Pusok, A., Kaus, B., & Popov, A. (2018, 05). The effect of rheological approximations in 3-d numerical simulations of subduction and collision. *Tectonophysics*, *746*, 296-311. doi: 10.1016/j.tecto.2018.04.017

Qiu, Q., Li, L., Hsu, Y.-J., Wang, Y., Chan, C.-H., & Switzer, A. D. (2019). Revised earthquake sources along manila trench for tsunami hazard assessment in the south china sea. *Natural Hazards and Earth System Sciences*, *19*(7), 1565–1583. doi: 10.5194/nhess-19-1565-2019

Rodríguez-González, J., Billen, M. I., & Negredo, A. M. (2014). Non-steady-state subduction and trench-parallel flow induced by overriding plate structure. *Earth and Planetary Science Letters*, *401*, 227-235. doi: 10.1016/j.epsl.2014.06.013

Royden, L. H., & Husson, L. (2006, 11). Trench motion, slab geometry and viscous stresses in subduction systems. *Geophysical Journal International*, *167*(2), 881-905. doi: 10.1111/j.1365-246X.2006.03079.x

Schellart, W. P. (2004). Kinematics of subduction and subduction-induced flow in the upper mantle. *Journal of Geophysical Research: Solid Earth*, *109*(B7). doi: 10.1029/2004JB002970

Schellart, W. P. (2008). Kinematics and flow patterns in deep mantle and upper mantle subduction models: Influence of the mantle depth and slab to mantle viscosity ratio. *Geochemistry, Geophysics, Geosystems*, *9*(3). doi: 10.1029/2007GC001656

Schellart, W. P., Freeman, J., Stegman, D., Moresi, L., & May, D. (2007, 03). Evolution and diversity of subduction zones controlled by slab width. *Nature*, *446*, 308-11. doi: 10.1038/nature05615

Sharples, W., Jadamec, M. A., Moresi, L. N., & Capitanio, F. A. (2014). Overriding plate controls on subduction evolution. *Journal of Geophysical Research: Solid Earth*, *119*(8), 6684-6704. doi: 10.1002/2014JB011163

Stegman, D., Farrington, R., Capitanio, F., & Schellart, W. (2010). A regime diagram for subduction styles from 3-d numerical models of free subduction. *Tectonophysics*, *483*(1), 29-45. (Convergent plate margin dynamics: New perspectives from structural geology, geophysics and geodynamic modelling) doi: 10.1016/j.tecto.2009.08.041

Stegman, D., Freeman, J., Schellart, W., Moresi, L., & May, D. (2006, 03). Influence of trench width on subduction hinge retreat rates in 3-d models of slab rollback. *Geochemistry Geophysics Geosystems*, *3060*. doi: 10.1029/2005GC001056

Strak, V., & Schellart, W. P. (2016). Control of slab width on subduction-induced upper mantle flow and associated upwellings: Insights from analog models. *Journal of Geophysical Research: Solid Earth*, *121*(6), 4641-4654. doi: 10.1002/2015JB012545

van Hunen, J., & Allen, M. B. (2011). Continental collision and slab break-off: A comparison of 3-d numerical models with observations. *Earth and Planetary Science Letters*, *302*(1), 27-37. doi: 10.1016/j.epsl.2010.11.035

Xue, K., Schellart, W. P., & Strak, V. (2020). Effect of plate length on subduction kinematics and slab geometry: Insights from buoyancy-driven analog subduction models. *Journal of Geophysical Research: Solid Earth*, *125*(11), e2020JB020514. doi: 10.1029/2020JB020514

Yamato, P., Husson, L., Braun, J., Loiselet, C., & Thieulot, C. (2009, 04). Influence of surrounding plates on 3d subduction dynamics. *Geophysical Research Letters - GEOPHYS RES LETT*, *36*, L07303. doi: 10.1029/2008GL036942

Čížková, H., & Bina, C. R. (2013). Effects of mantle and subduction-interface rheologies on slab stagnation and trench rollback. *Earth and Planetary Science Letters*, *379*, 95-103. doi: 10.1016/j.epsl.2013.08.011

Čížková, H., & Bina, C. R. (2019). Linked influences on slab stagnation: Interplay between lower mantle viscosity structure, phase transitions, and plate coupling. *Earth and Planetary Science Letters*, *509*, 88-99. doi: 10.1016/j.epsl.2018.12.027

Supporting Information for

Overriding plate thickness as a controlling factor for trench retreat rates in narrow subduction zones

Pedro J. Gea[1,2], Flor de Lis Mancilla[1,2], Ana M. Negredo[3,4], and Jeroen van Hunen[5]

[1]Department of Theoretical Physics and Cosmology, University of Granada, Granada, Spain
[2]Andalusian Institute of Geophysics, University of Granada, Granada, Spain
[3]Department of Earth Physics and Astrophysics, Complutense University of Madrid, Madrid, Spain
[4]Institute of Geosciences IGEO (CSIC, UCM), Madrid, Spain
[5]Department of Earth Sciences, Durham University, DH1 3LE Durham, UK

Contents of this file

1. Text S1 to S2

2. Figures S1 to S2

3. Tables S1 to S3

Introduction

Text S1 describes the basic equations and Text S2 summarizes the rheological model. Figure S1 shows an example of model evolution for a slab width of 600 km. Figure S2 ilustrates the effect of the viscous coupling at the lateral slab edge on trench geometry. Table S1 contains the model parameters used in the numerical simulations. Tabla S2 summarizes the parameters tested in the numerical experiments. Table S3 includes the data used in Figure 4 with their references.

Text S1. Numerical method

We use version 2.4.0 of the finite-element code ASPECT (Advanced Solver for Problems in Earth's ConvecTion) (Kronbichler et al., 2012; Heister et al., 2017; Gassmöller et al., 2018; Bangerth et al., 2021a, 2021b) to simulate 3D self-consistent subduction models. The momentum, mass, and energy conservation equations for an incompressible fluid are solved using the Boussinesq approximation:

$$\nabla \cdot \mathbf{u} = 0 \tag{1}$$

$$-\nabla \cdot 2\mu\dot{\varepsilon}\left(\mathbf{u}\right) + \nabla P = \rho\mathbf{g} \tag{2}$$

$$\rho_o c_p \left(\frac{\partial T}{\partial t} + \mathbf{u} \cdot \nabla T\right) - \nabla \cdot k\nabla T = \rho_o H \tag{3}$$

where $\dot{\varepsilon} = \frac{1}{2}\left(\nabla\mathbf{u} + \nabla\mathbf{u}^T\right)$ is the strain rate tensor, ρ is the density, μ is the viscosity, P is the pressure, $\mathbf{u}$ is the velocity, $\mathbf{g}$ is the gravitational acceleration, c_p is the specific heat, T is the temperature, k is the thermal conductivity, ρ_o is the density at a reference temperature T_o and H is the radiogenic heating, which is neglected in our models.

Besides these equations, ASPECT solves the advection of compositional fields c_i, which are used to track materials and their properties throughout the simulations:

$$\frac{\partial c_i}{\partial t} + \mathbf{u} \cdot \nabla c_i = 0 \tag{4}$$

Text S2. Rheological model

We use a temperature-dependent rheology in which the viscosity is given by:

$$\mu = \frac{1}{2A} d^m \exp\left(\frac{E + PV}{RT}\right) \quad (5)$$

where A is a prefactor of the equation, d is the grain size, m is the grain size exponent, E is the activation energy, V is the activation volume, P is the pressure and R is the gas constant.

For the upper mantle (asthenosphere and lithosphere) we use rheological parameters from wet olivine (Hirth & Kohlstedt, 2003). With these parameters, we obtain a viscosity of $1.57 \cdot 10^{20}$ Pa s at a depth of 150 km. For the overriding plate crust we adopt rheological parameters from wet anorthite feldspar (Bürgmann & Dresen, 2008). The temperature-dependent viscosity is capped by a preset minimum and a maximum viscosity of 10^{19} and $1.57 \cdot 10^{23}$ Pa s respectively to avoid large viscosity jumps. For the oceanic crust, we adopt a low constant viscosity of 10^{20} Pa s to decouple the slab from the top surface and the overriding plate (OP) and to facilitate subduction. A low viscosity of 10^{20} Pa s is also used in the weak layer as a weak mechanical coupling of the subducting and overriding plates with the lateral plate. The effects of varying this viscosity is shown in Figures 2e and S2. All model parameters are listed in table S1.

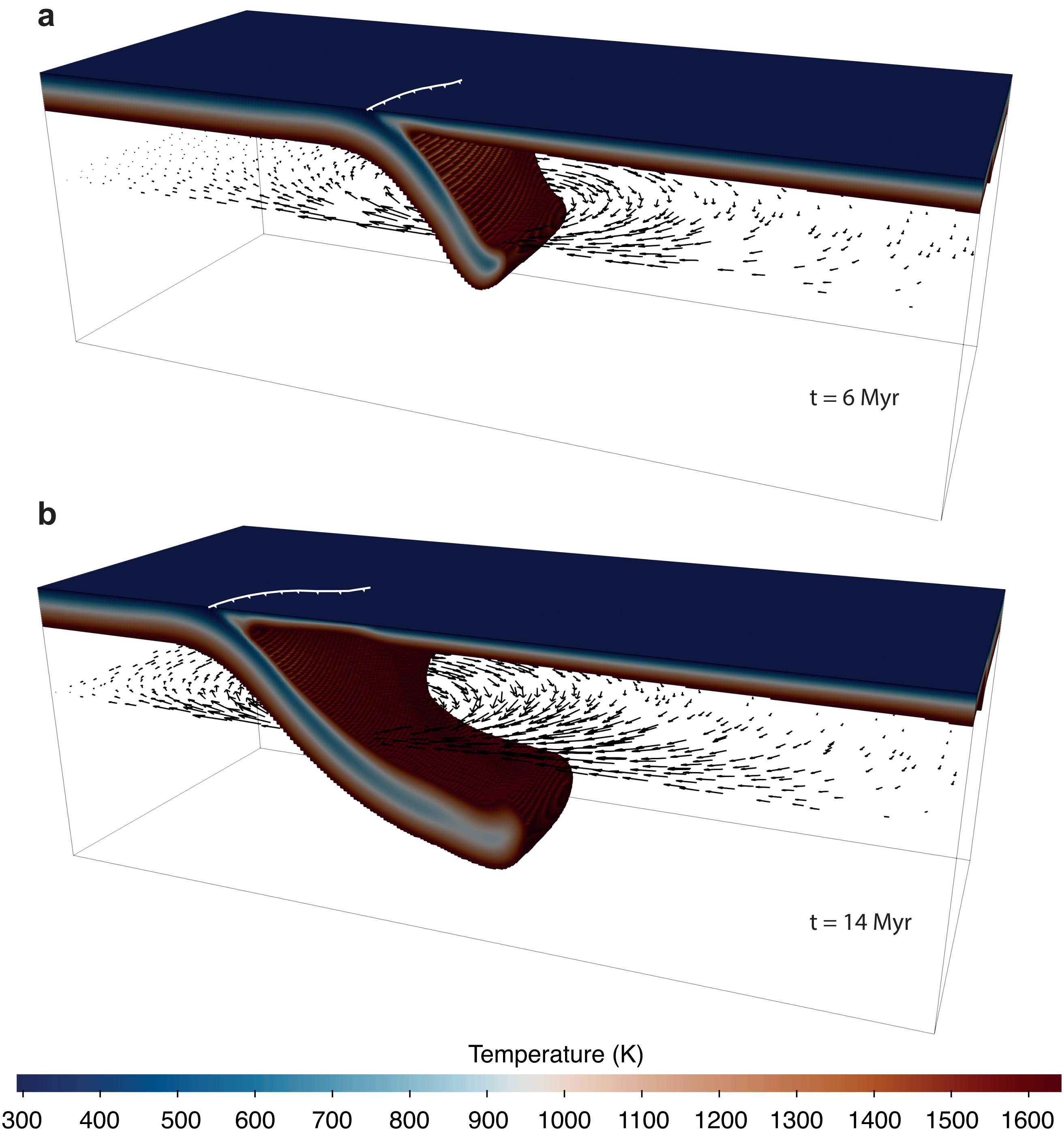

Figure S1. 3D perspective view of the subduction zone with the temperature field displayed for (a) 6 Myr and (b) 14 Myr. The figures are cutouts of the temperature between 293 K and 1500 K. White lines with triangles on the surface mark the trench position. Black arrows show the horizontal velocity field around the slab at 250 km depth.

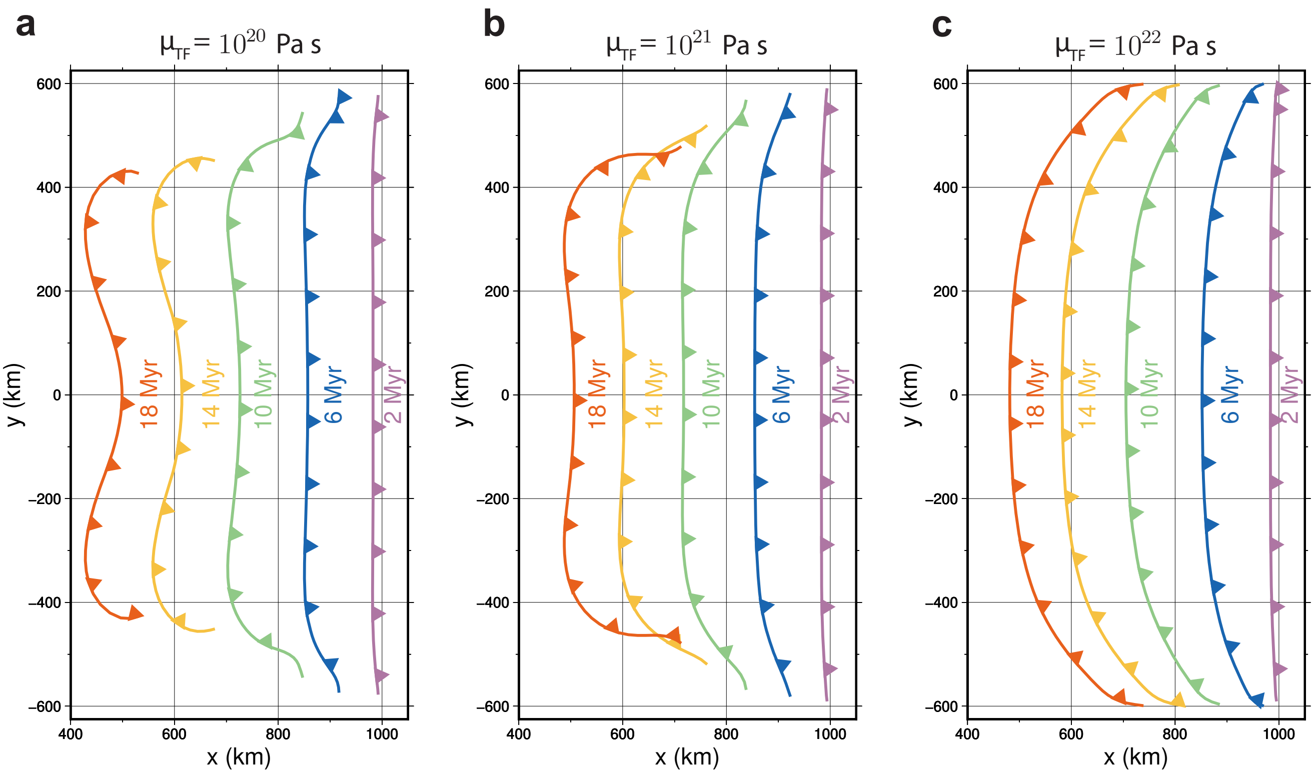

Figure S2. Evolution of the subduction trench for transform fault viscosities of (a) 10^{20} Pa s, (b) 10^{21} Pa s and (a) 10^{22} Pa s. The results shown correspond to models with overriding plate thicknesses of 70 km and slab widths of 1200 km (experiments 5, 10 and 15 in table S2).

Table S1. Model parameters

Symbol	Parameter name	Value	Units
Lithosphere and mantle rheology			
A	Exponential prefactor	$5.973 \cdot 10^{-16}$	$\mathrm{Pa^{-1}\,m^3\,s^{-1}}$
E	Activation energy	335	$\mathrm{kJ\,mol^{-1}}$
V	Activation volume	$4 \cdot 10^{-6}$	$\mathrm{m^3\,mol^{-1}}$
d	Grain size	10^{-2}	m
m	Grain size exponent	3	-
Overriding plate crust rheology			
A	Exponential prefactor	$5 \cdot 10^{-11}$	$\mathrm{Pa^{-1}\,m^3\,s^{-1}}$
E	Activation energy	170	$\mathrm{kJ\,mol^{-1}}$
V	Activation volume	0	-
d	Grain size	10^{-2}	m
m	Grain size exponent	3	-
Other model parameters			
ρ_{um}	Upper mantle density	3300	$\mathrm{kg\,m^{-3}}$
ρ_{lc}	Overriding plate crust density	2900	$\mathrm{kg\,m^{-3}}$
ρ_{oc}	Oceanic crust density	3300	$\mathrm{kg\,m^{-3}}$
ρ_{TF}	Transform fault density	3300	$\mathrm{kg\,m^{-3}}$
μ_{oc}	Oceanic crust viscosity	10^{20}	Pa s
μ_{TF}	Transform fault viscosity	10^{20}	Pa s
μ_{min}	Minimum viscosity	10^{19}	Pa s
μ_{max}	Maximum viscosity	$1.57 \cdot 10^{23}$	Pa s
c_p	Specific heat	1250	$\mathrm{J\,kg^{-1}\,K^{-1}}$
κ	Thermal diffusivity	$0.8 \cdot 10^{-6}$	$\mathrm{m^2\,s^{-1}}$
α	Thermal expansion coefficient	$3.5 \cdot 10^{-5}$	$\mathrm{K^{-1}}$
R	Gas constant	8.31	$\mathrm{J\,K^{-1}\,mol^{-1}}$
g	Gravitational acceleration	9.8	$\mathrm{m\,s^{-2}}$
T_0	Reference temperature	293	K

Table S2. Parameters examined in the numerical models

Experiment	**W/2 (km)**	**W (km)**	**OP thickness (km)**	$\boldsymbol{\mu_{TF}}$(**Pa** · s)
1	200	400	70	10^{20}
2	300	600	70	10^{20}
3	400	800	70	10^{20}
4	500	1000	70	10^{20}
5	600	1200	70	10^{20}
6	200	400	70	10^{21}
7	300	600	70	10^{21}
8	400	800	70	10^{21}
9	500	1000	70	10^{21}
10	600	1200	70	10^{21}
11	200	400	70	10^{22}
12	300	600	70	10^{22}
13	400	800	70	10^{22}
14	500	1000	70	10^{22}
15	600	1200	70	10^{22}
16	300	600	40	10^{20}
17	300	600	50	10^{20}
18	300	600	60	10^{20}
19	300	600	80	10^{20}
20	300	600	90	10^{20}
21	300	600	100	10^{20}

Table S3. Data for narrow subduction zones used in Figures 4D and 4E. The subduction zone width (W) and trench retreat velocity (V_T) have been obtained from Schellart et al. (2007) (references therein). The overriding plate (OP) thickness has been obtained from different regional studies.

Subduction system	**W (km)**	V_T **(cm/yr)**	**OP thickness (km)**	**Reference OP thickness**
Gibraltar	250	0.9	100	Molina-Aguilera et al. (2019)*
Calabria	300	6.8	50	Rosenbaum and Lister (2004)
South Shetland	450	3.1	70	Parera-Portell et al. (2021)
Halmahera	500	7	50	Zhang et al. (2017)†
North Sulawesi	500	1.3	75	Dong et al. (2022)†§
Puysegur	750	4.2	59	Shuck et al. (2021)‡
Scotia	800	5.7	70	Fullea et al. (2021)¶
Sangihe	850	2.2	100	Fan and Zhao (2018)‖
Trobriand	900	7.6	55	Martinez et al. (2001)
Makran	900	0.2	90	Motaghi et al. (2020)
Manila	1000	5.7	80	Fullea et al. (2021)¶

*This value is obtained for the West Alboran Basin, near the trench.

†Based on numerical modelling.

§Models with OP 75 km thick best fit heat flux observations.

‡assuming that the crustal stretching factor β=1.7 obtained by Shuck et al. (2021) for the Solander basin stands for the entire lithosphere.

¶Temptatively from WinterC.

‖This value was also tested in the models of Zhang et al. (2017).

References From the Supporting Information

Bürgmann, R., & Dresen, G. (2008). Rheology of the lower crust and upper mantle: Evidence from rock mechanics, geodesy, and field observations. *Annual Review of Earth and Planetary Sciences*, *36*(1), 531-567. doi: 10.1146/annurev.earth.36.031207.124326

Dong, M., Lü, C., Zhang, J., & Hao, T. (2022). Downgoing plate-buoyancy driven retreat of north sulawesi trench: Transition of a passive margin into a subduction zone. *Geophysical Research Letters*, *49*(23), e2022GL101130. (e2022GL101130 2022GL101130) doi: 10.1029/2022GL101130

Fan, J., & Zhao, D. (2018). Evolution of the southern segment of the philippine trench: Constraints from seismic tomography. *Geochemistry, Geophysics, Geosystems*, *19*(11), 4612-4627. doi: 10.1029/2018GC007685

Fullea, J., Lebedev, S., Martinec, Z., & Celli, N. L. (2021, 03). WINTERC-G: mapping the upper mantle thermochemical heterogeneity from coupled geophysical–petrological inversion of seismic waveforms, heat flow, surface elevation and gravity satellite data. *Geophysical Journal International*, *226*(1), 146-191. doi: 10.1093/gji/ggab094

Hirth, G., & Kohlstedt, D. (2003, 01). Rheology of the upper mantle and the mantle wedge: A view from the experimentalists. *Washington DC American Geophysical Union Geophysical Monograph Series*, *138*, 83-105. doi: 10.1029/138GM06

Martinez, F., Goodliffe, A., & Taylor, B. (2001, 07). Metamorphic core complex formation by density inversion and lower-crust extrusion. *Nature*, *411*, 930-4. doi: 10.1038/35082042

Molina-Aguilera, A., de Lis Mancilla, F., Morales, J., Stich, D., Yuan, X., & Heit, B. (2019, 01). Connection between the Jurassic oceanic lithosphere of the Gulf of Cádiz and the Alboran slab imaged by Sp receiver functions. *Geology*, *47*(3), 227-230. doi: 10.1130/G45654.1

Motaghi, K., Shabanian, E., & Nozad-Khalil, T. (2020). Deep structure of the western coast of the makran subduction zone, se iran. *Tectonophysics*, *776*, 228314. doi: 10.1016/j.tecto.2019.228314

Parera-Portell, J. A., de Lis Mancilla, F., Morales, J., Almendros, J., & Jiménez-Morales, V. (2021). Structure of the crust and upper mantle beneath the bransfield strait (antarctica) using p receiver functions. *Tectonophysics*, *802*, 228744. doi: 10.1016/j.tecto.2021.228744

Rosenbaum, G., & Lister, G. S. (2004). Neogene and quaternary rollback evolution of the tyrrhenian sea, the apennines, and the sicilian maghrebides. *Tectonics*, *23*(1). doi: 10.1029/2003TC001518

Shuck, B., Van Avendonk, H., Gulick, S. P. S., Gurnis, M., Sutherland, R., Stock, J., ... Hess, T. (2021). Strike-slip enables subduction initiation beneath a failed rift: New seismic constraints from puysegur margin, new zealand. *Tectonics*, *40*(5), e2020TC006436. (e2020TC006436 2020TC006436) doi: 10.1029/2020TC006436

Zhang, Q., Guo, F., Zhao, L., & Wu, Y. (2017). Geodynamics of divergent double subduction: 3-d numerical modeling of a cenozoic example in the molucca sea region, indonesia. *Journal of Geophysical Research: Solid Earth*, *122*(5), 3977-3998. doi: 10.1002/2017JB013991